Supporting Information

Helical Counter-Directional Migration-Induced Solvation Sheath Constructing Reinforced Electrode-Electrolyte Interphases for Ultra-Stable Anode-Free Lithium Metal Batteries

Yunyi Chen[1,2,3], Xitang Qian[1,2], Yuxiang Lyu[1,2], Yican Qiu[1,2], Yee Tung Kwan[1], Siyu Zhou[1,2], Xinyi Lan[1,2], Siqi Lu[1,2], Minhua Shao[1,2,3,4]*

1. Department of Chemical and Biological Engineering, The Hong Kong University of Science and Technology, Kowloon 999077 Hong Kong, China.
2. Energy Institute, The Hong Kong University of Science and Technology, Clear Water Bay, Kowloon, Hong Kong 999077, China.
3. Guangzhou Key Laboratory of Electrochemical Energy Storage Technologies, Guangzhou HKUST Fok Ying Tung Research Institute, Guangzhou 511458, China.
4. CIAC-HKUST Joint Laboratory for Hydrogen Energy, The Hong Kong University of Science and Technology, Clear Watery Bay, Kowloon, Hong Kong 999077, China.
5. *Corresponding to email: kemshao@ust.hk

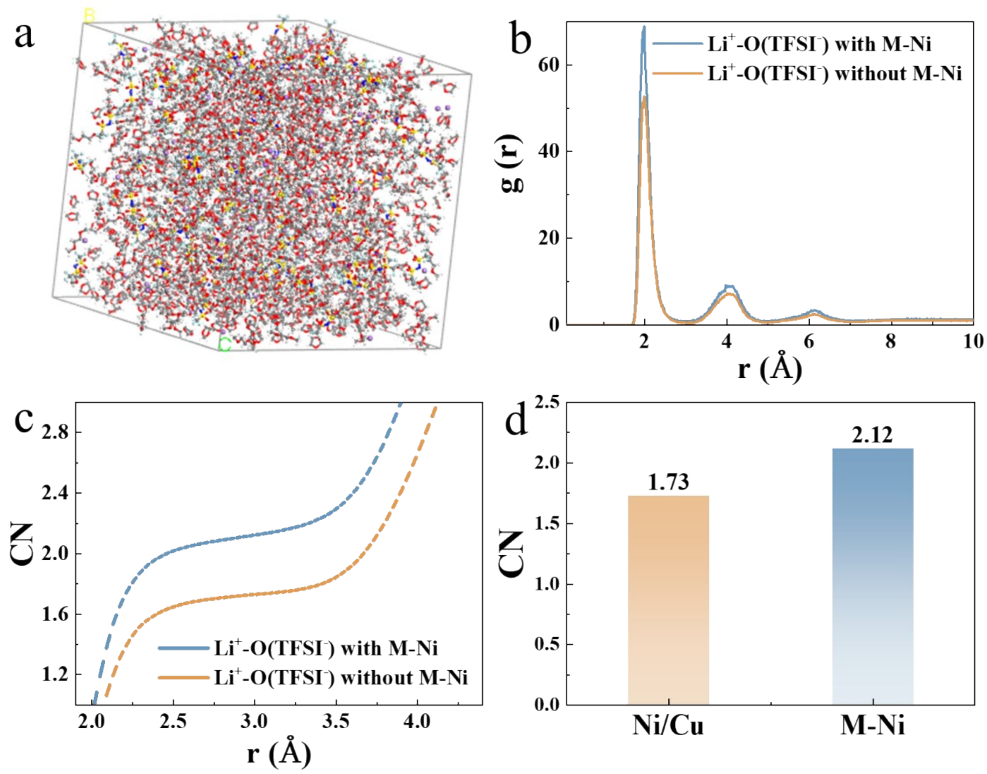

Figure S1. MD simulation of solvation sheath. a) Snapshot of the simulation box, b) RDFs of cation-anion [Li^+-O(Li^+/$TFSI^-$)] with or without ILF, c,d) CN of cation-anion [Li^+-O(Li^+/$TFSI^-$)] with or without ILF.

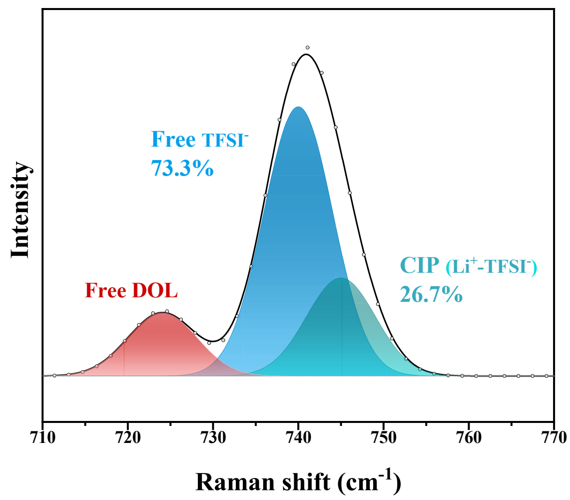

Figure S2. Raman spectra of $TFSI^-$ with Cu foil.

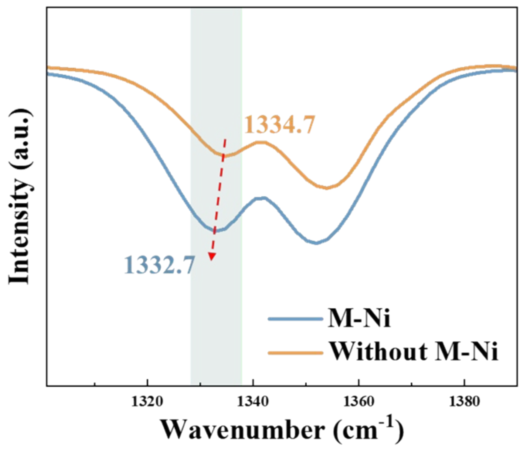

Figure S3. FTIR spectra of $TFSI^-$ bond in different samples (with or without M-Ni).

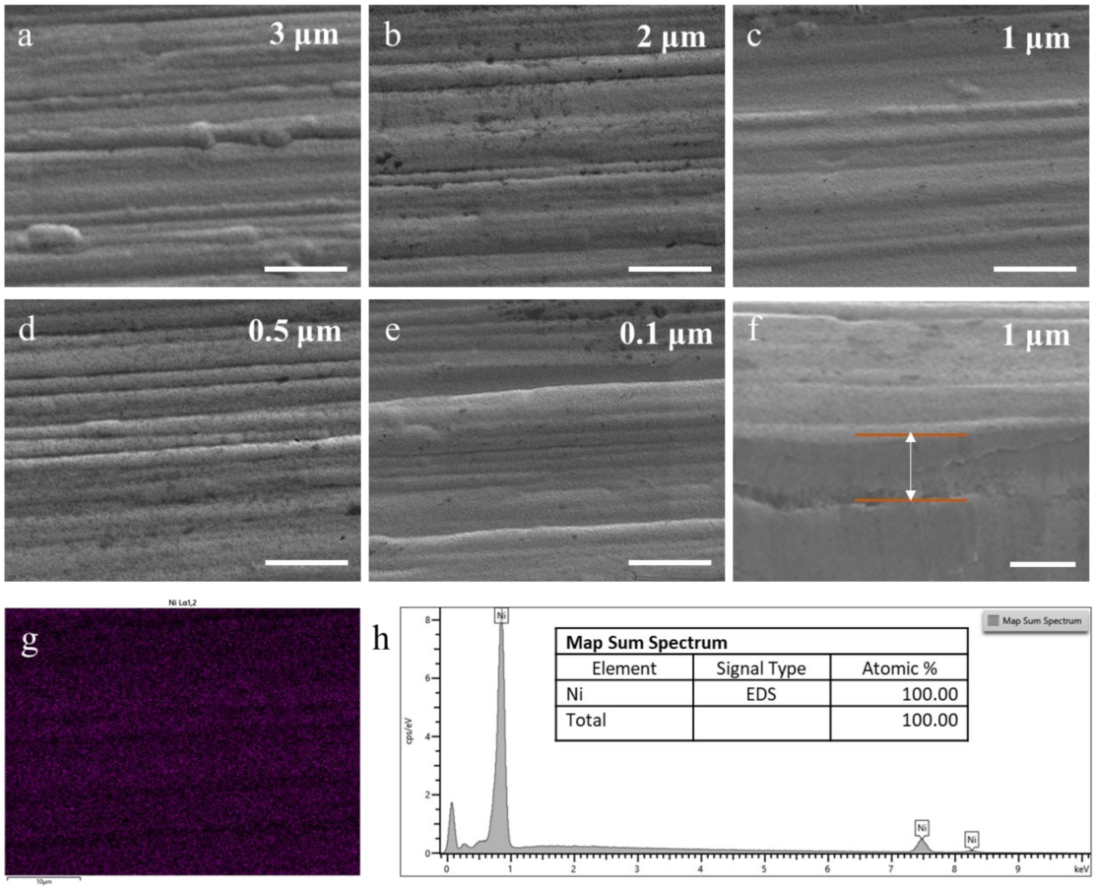

Figure S4. a-e) SEM images of Cu@Ni foils with various M-Ni-layer thickness. f) Cross-section of nickel coated copper foil. g) EDS mapping and spectrum of the current collector with M-Ni.

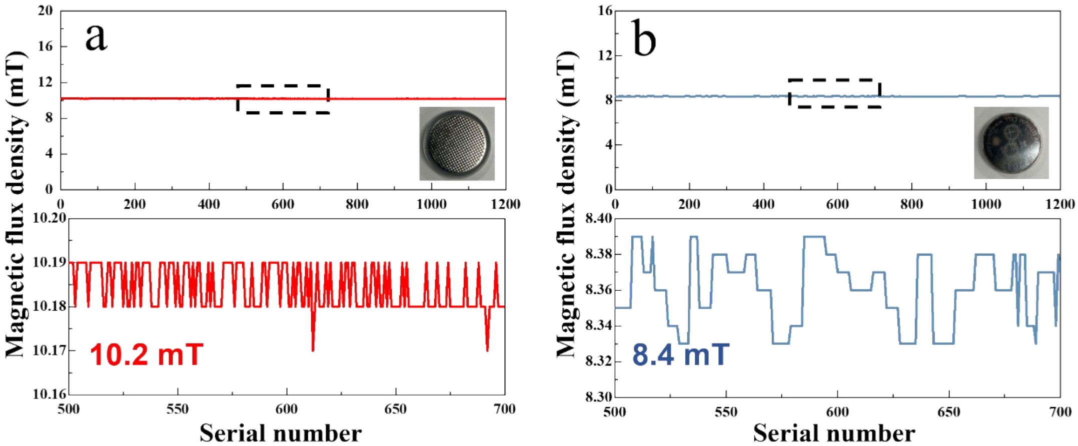

Figure S5. The quantitative data for the strength of magnetic field from M-Ni. (a) Anode side, (b) Cathode side.

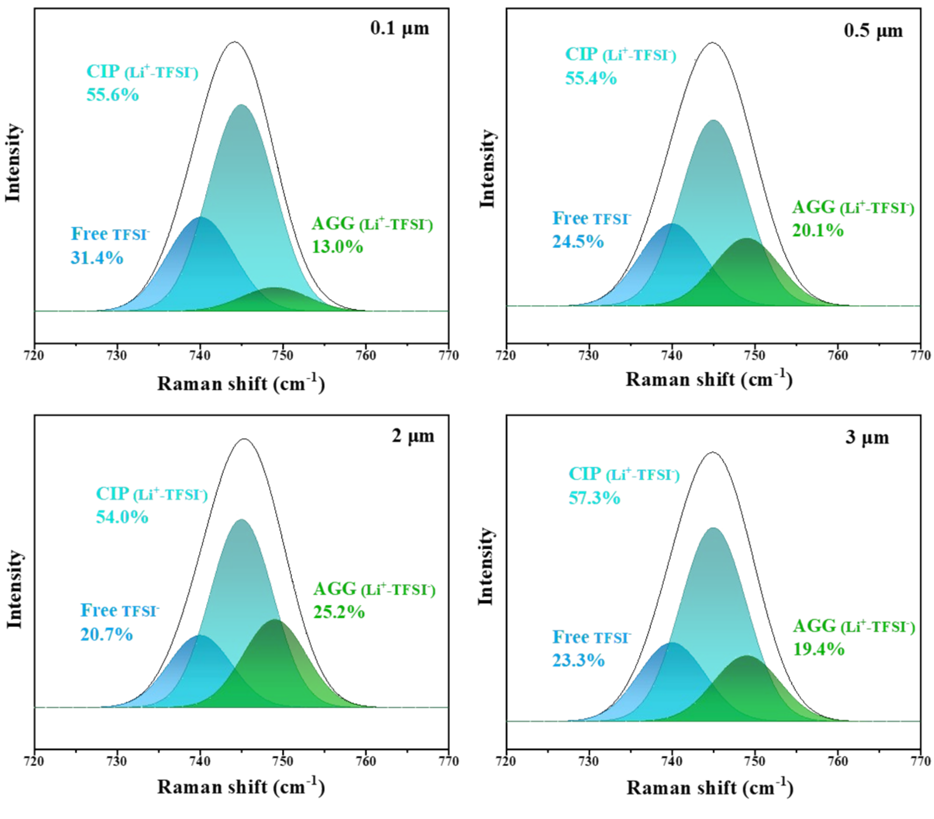

Figure S6. Raman spectra of $TFSI^-$ with various M-Ni-layer thickness.

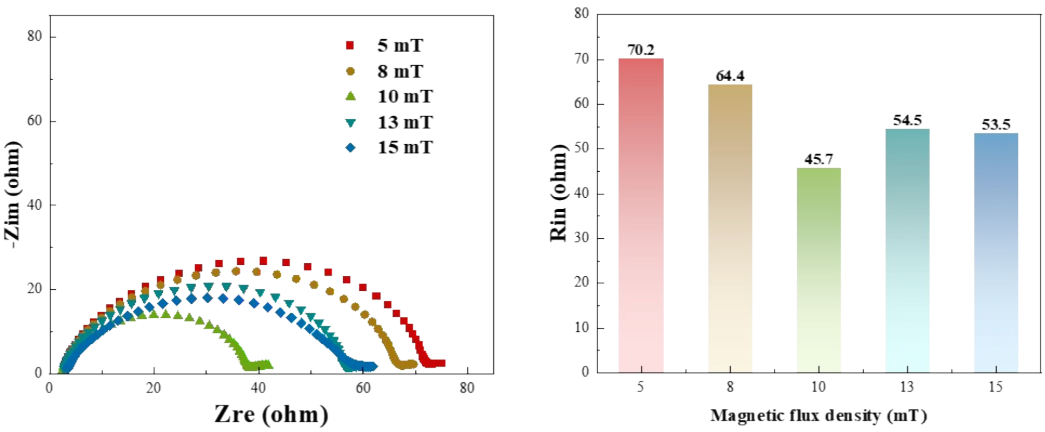

Figure S7. Electrochemical impedance spectra (EIS) and Impedance comparison of M-Ni-layer with various magnetic flux densities (0.1μm-5mT, 0.5μm-8mT, 1μm-10mT, 2μm-13mT, 3μm-15mT).

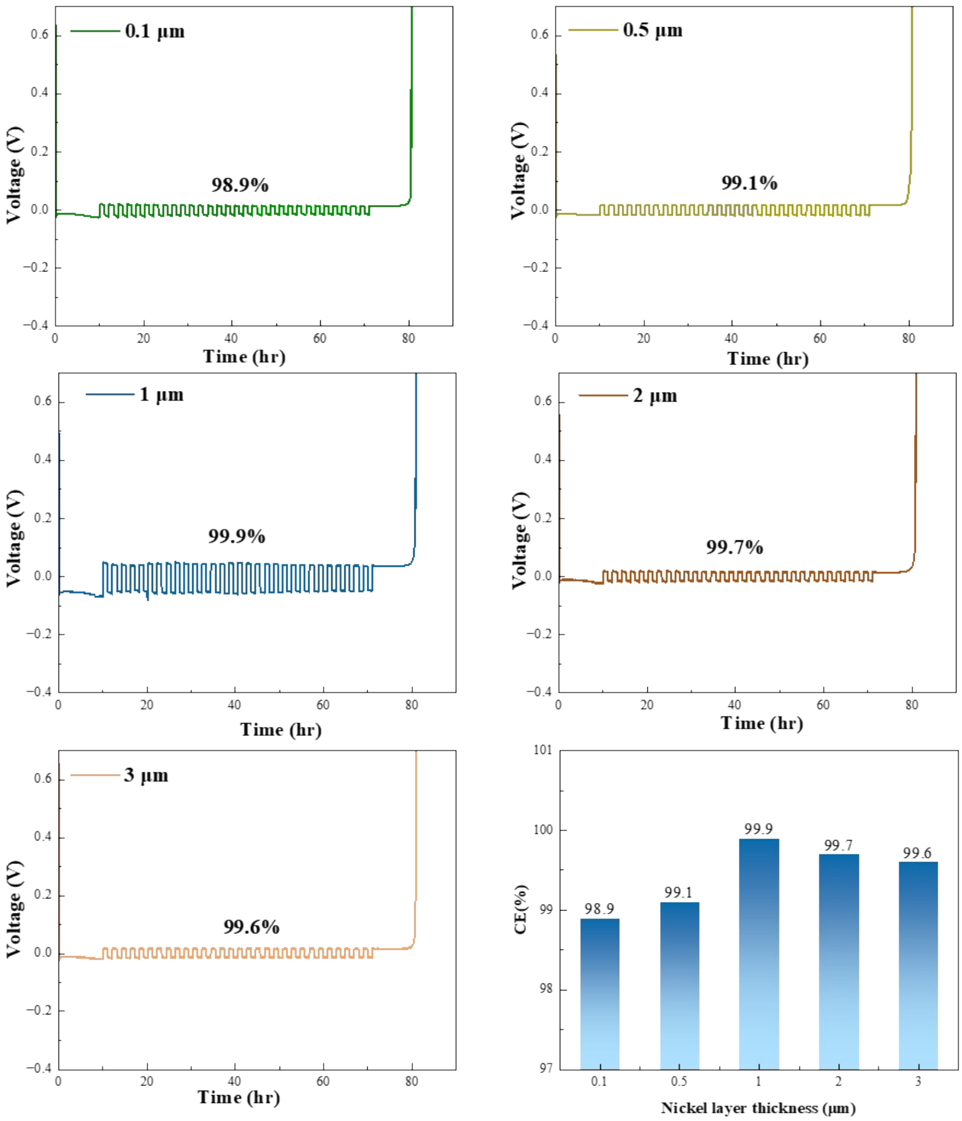

Figure S8. Average coulombic efficiency of Li|Cu cells with different M-Ni-layer thickness.

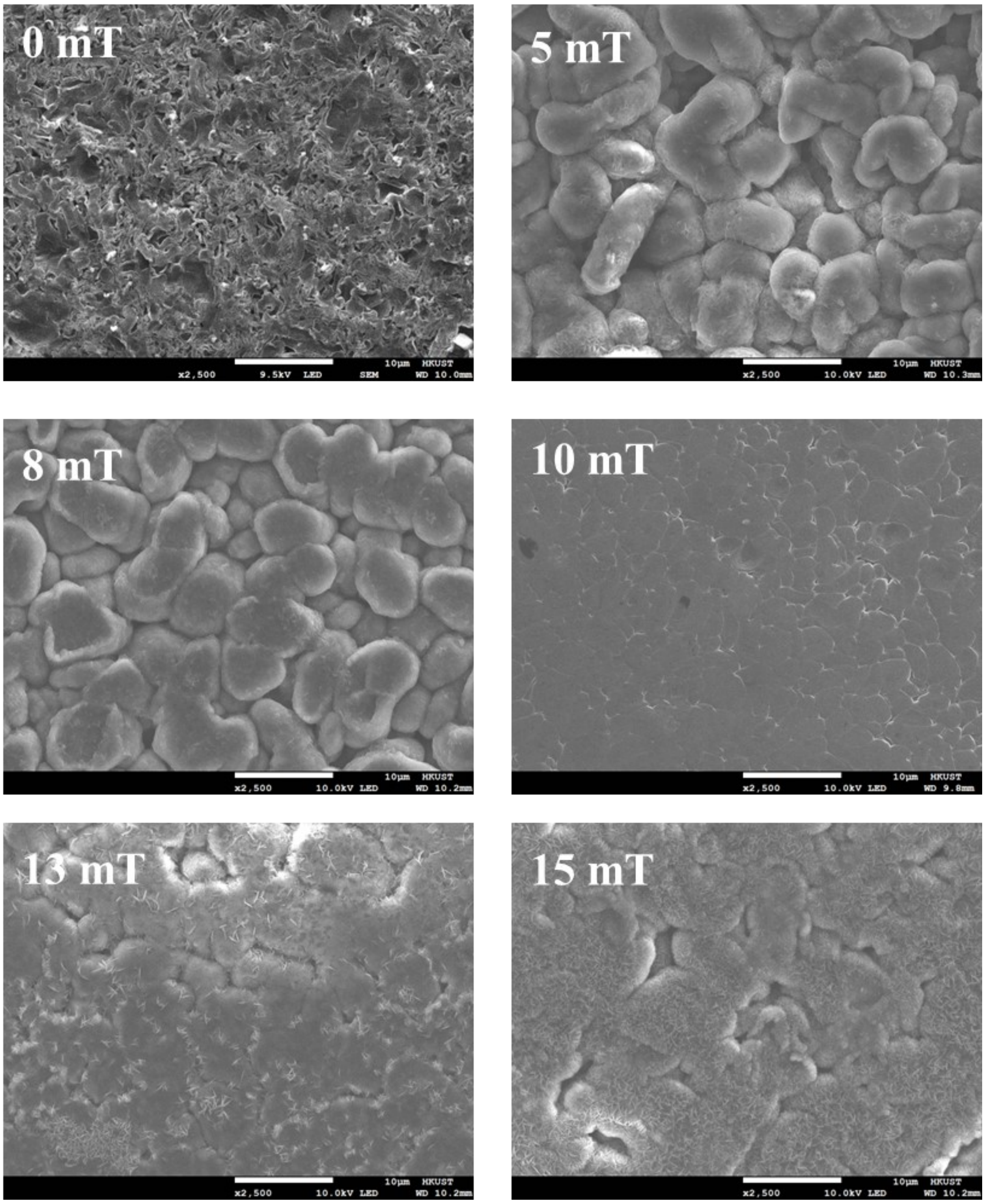

Figure S9. Lithium deposition morphologies with different M-Ni-layer thickness and magnetic flux densities (0.1μm-5mT, 0.5μm-8mT, 1μm-10mT, 2μm-13mT, 3μm-15mT).

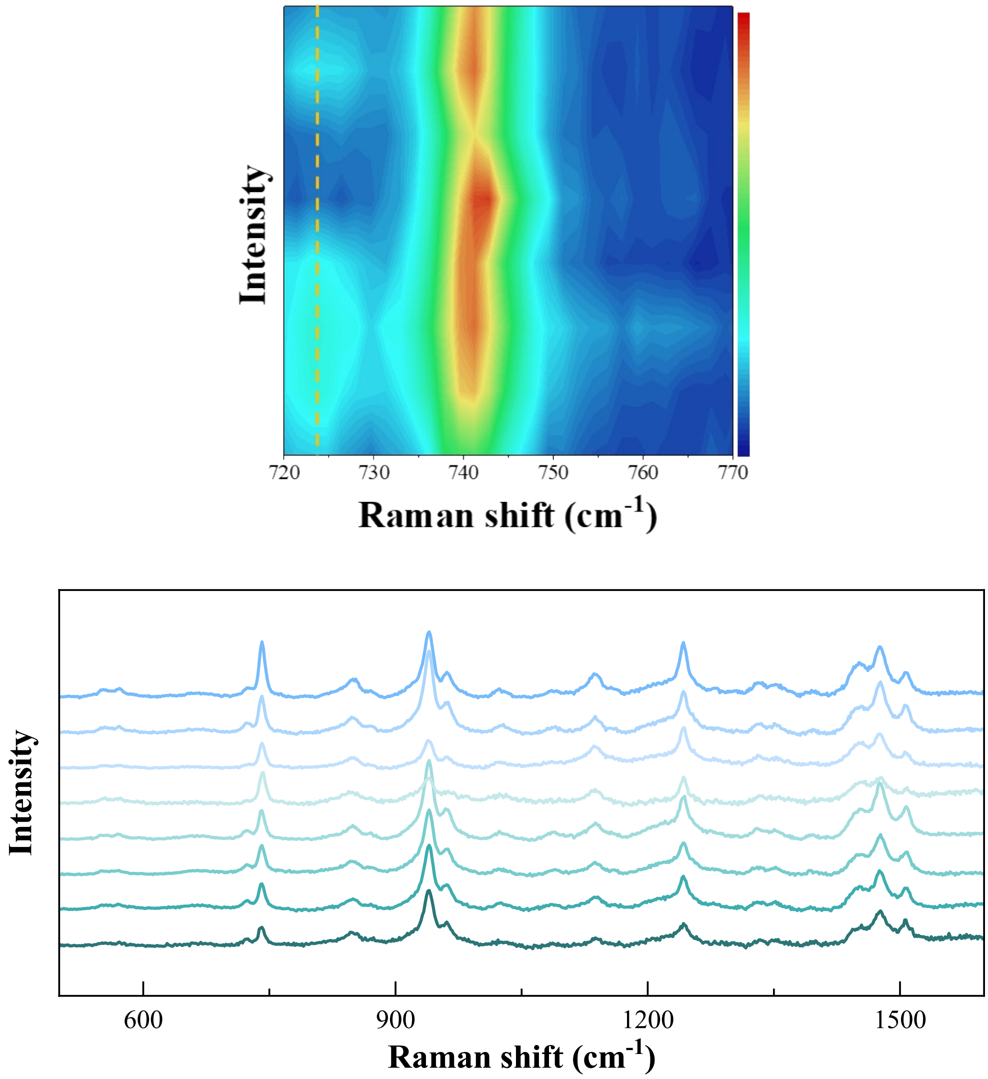

Figure S10. In-situ Raman spectra of $TFSI^-$ during cycles without M-Ni, and In-situ Raman curves during charging discharging cycles with without M-Ni.

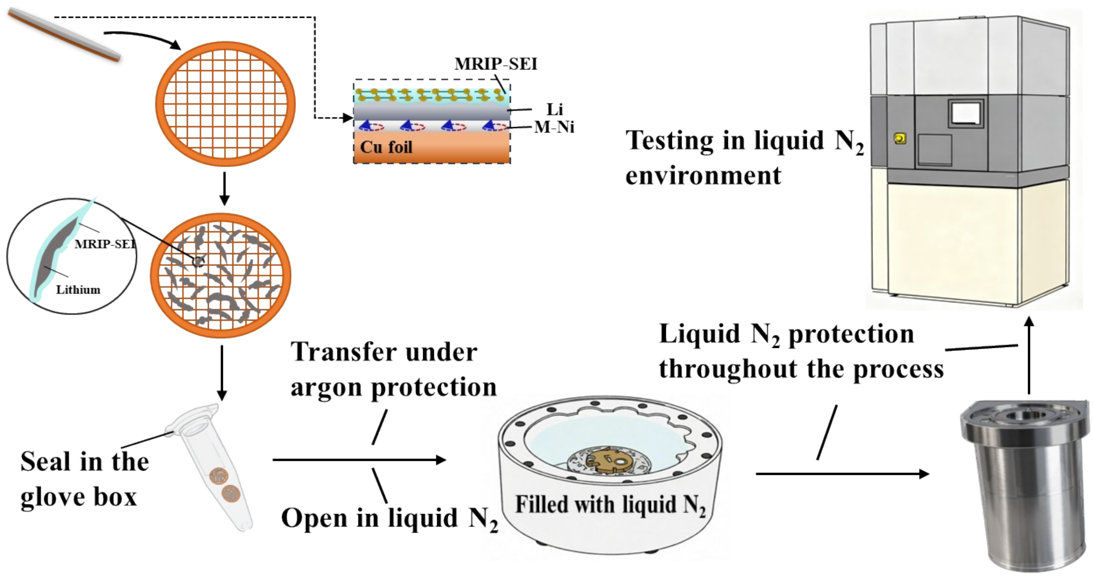

Figure S11. Schematic diagram of sample preparation and testing process for Cryo-TEM characterization.

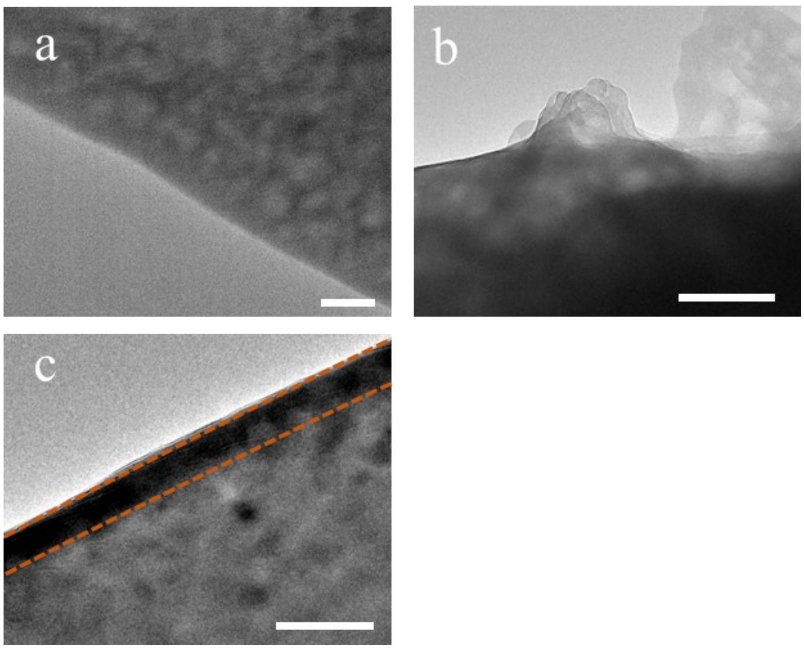

Figure S12. a) High-resolution Cryo-TEM images of the OSS-SEI (Scale bar: 10 nm). Cryo-TEM images of b) Ni-SEI and c) MRIP-SEI after charge/discharge cycles (Scale bar: 50 nm).

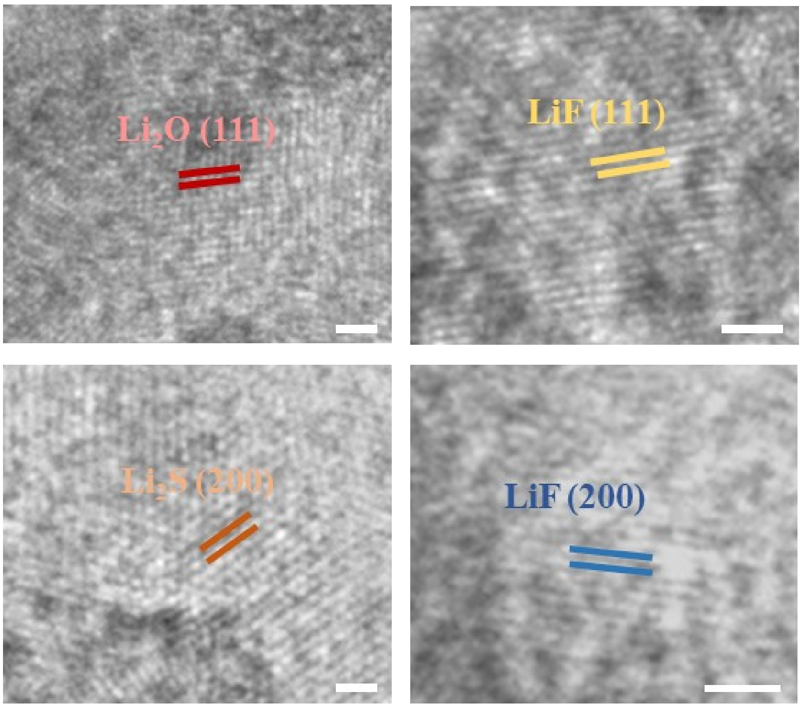

Figure S13. Cryo-EM images of magnification revealing lattice fringes corresponding to LiF (111), LiF (200), Li_2S (200), and Li_2O (111) in MRIP-SEI (Scale bar: 1 nm).

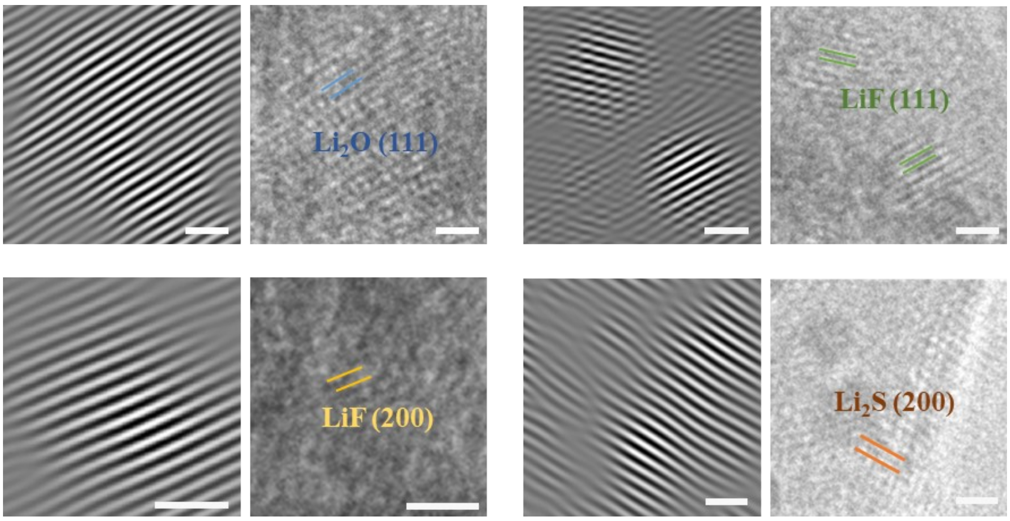

Figure S14. Cryo-EM images and inverse FFT images of magnification revealing lattice fringes corresponding to LiF (111), LiF (200), Li_2S (200), and Li_2O (111) in MRIP-SEI after cycling tests (Scale bar: 1 nm).

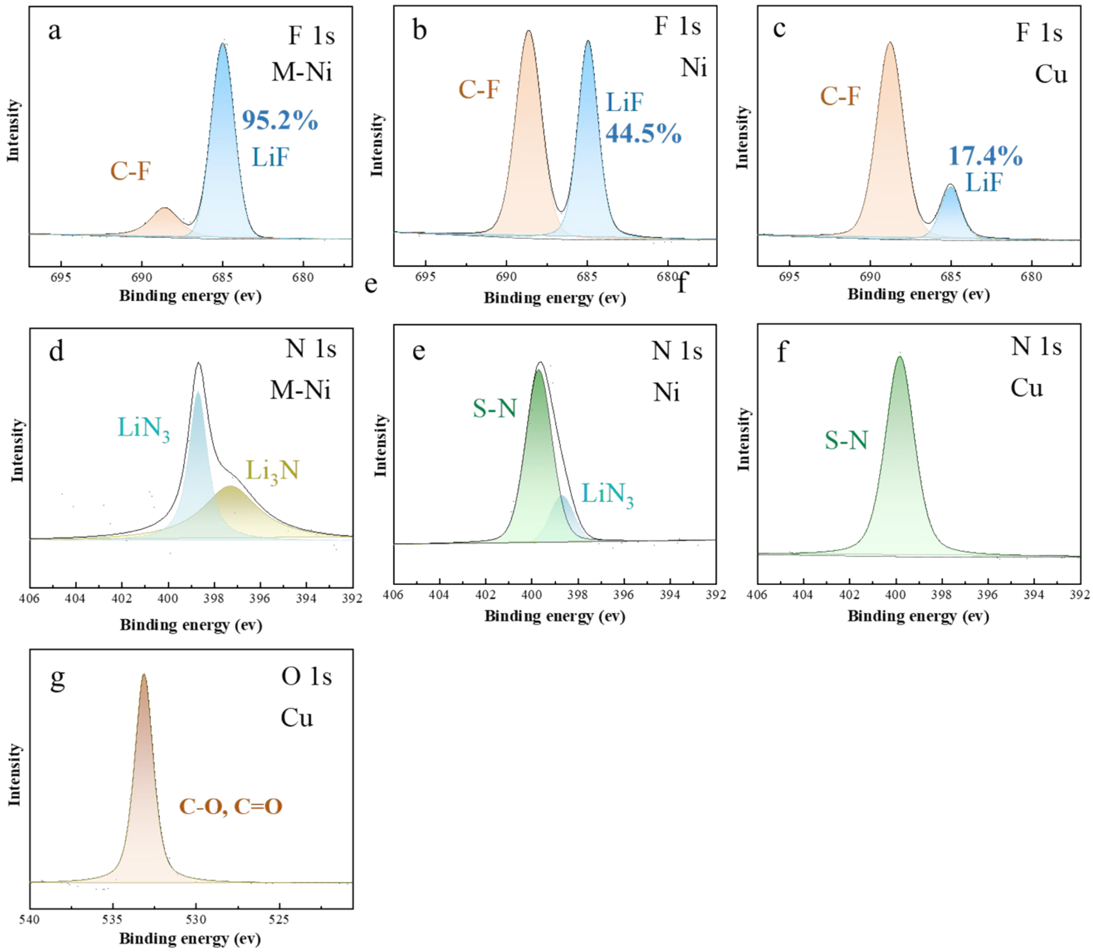

Figure S15. a-c) XPS spectra of F 1s of a) MRIP-SEI, b) Ni-SEI, and c) Cu-SEI. d-f) XPS spectra of N 1s of d) MRIP-SEI, e) Ni-SEI, and f) Cu-SEI. g) XPS spectra of O 1s of Cu-SEI.

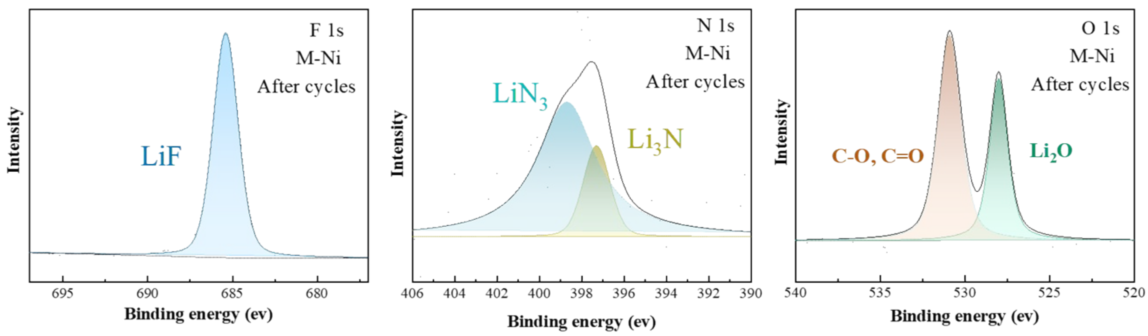

Figure S16. XPS spectra of MRIP-SEI (using M-Ni) after charge-discharge cycling test.

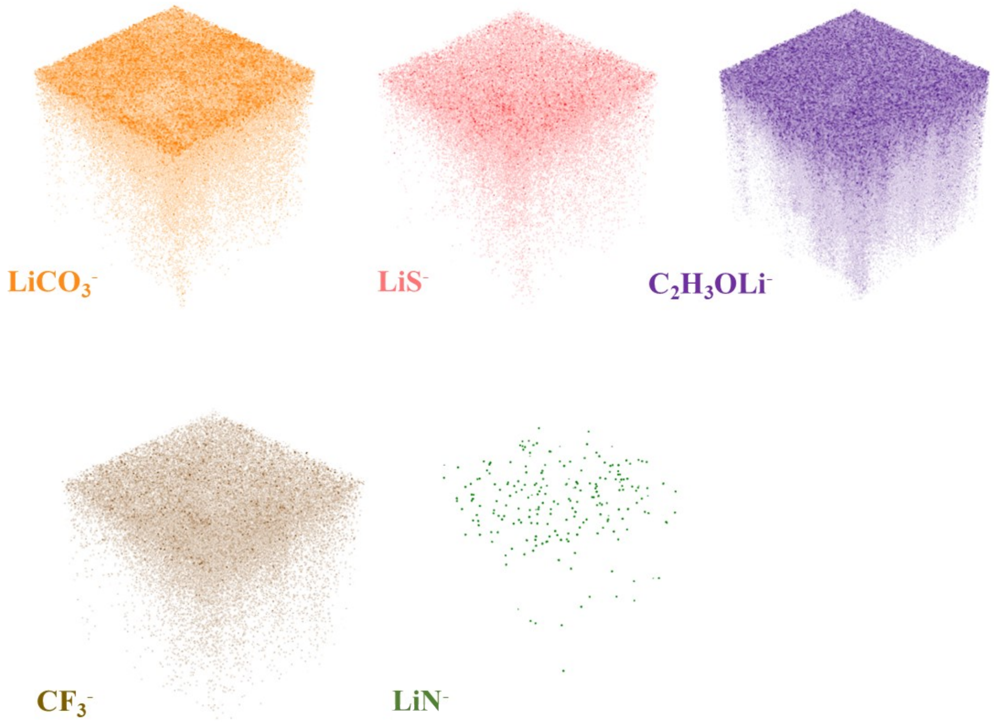

Figure S17. TOF-SIMS 3D distribution of Ni-SEI.

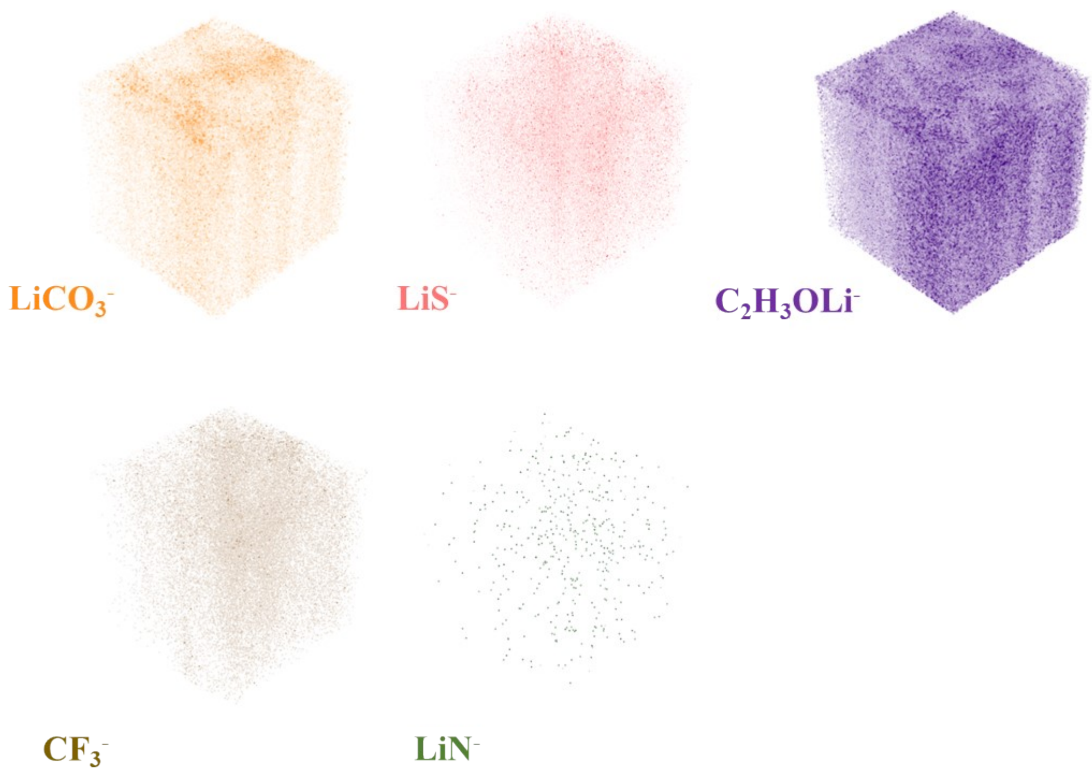

Figure S18. TOF-SIMS 3D distribution of Cu-SEI.

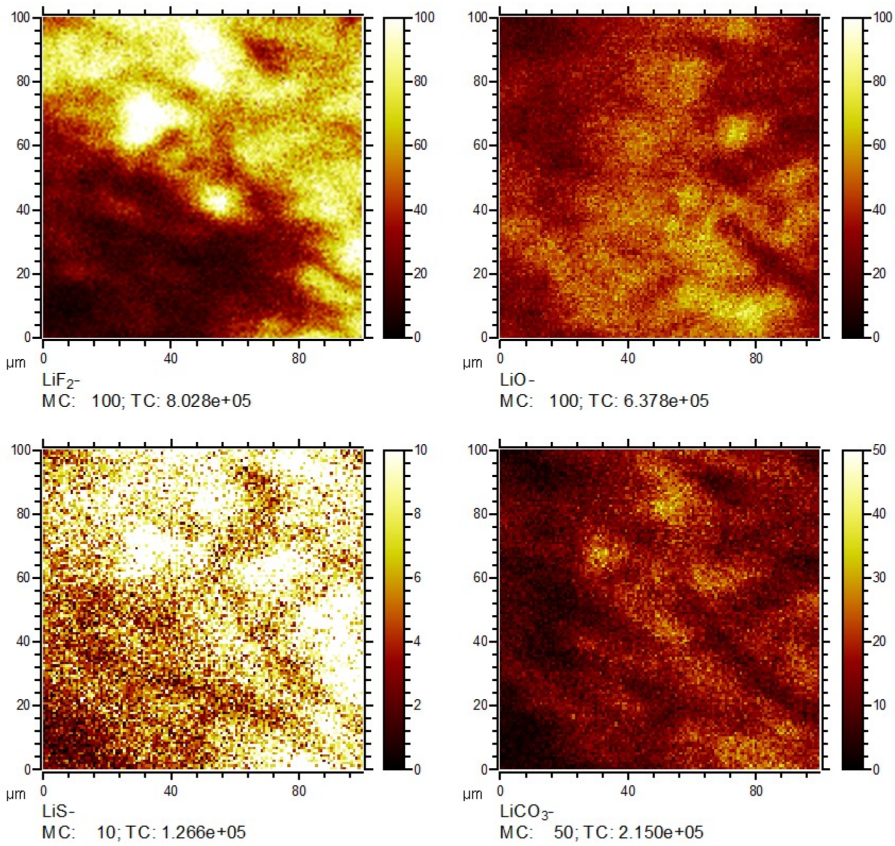

Figure S19. Single-color gradient maps of LiF_2-, $LiCO_3^-$, LiS^-, and LiO^- of Cu-SEI.

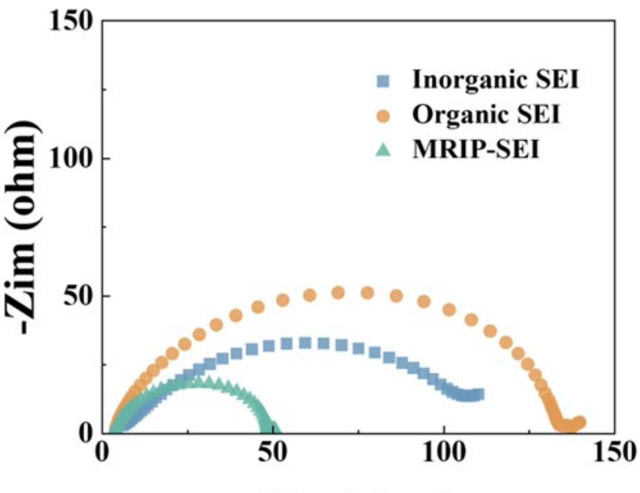

Figure S20. EIS data of MRIP-SEI, Inorganic-SEI, and Organic-SEI (Cu-SEI).

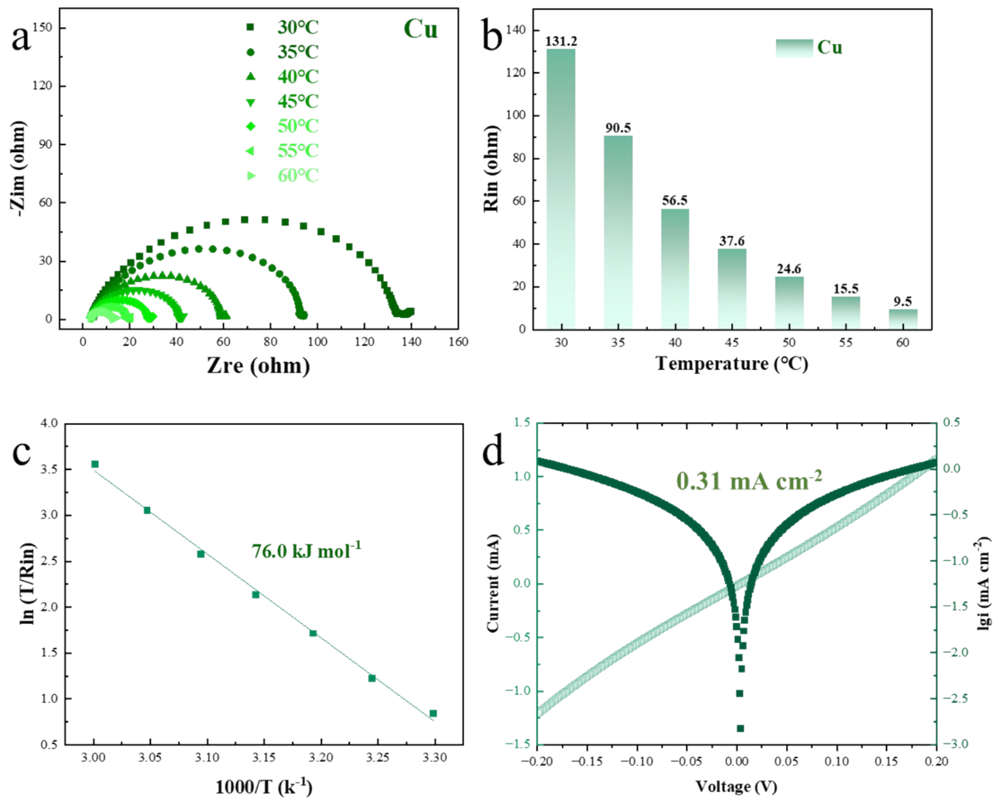

Figure S21. a) Electrochemical impedance spectra (EIS) after the generation of SEI with Cu at seven different temperatures (30, 35, 40, 45, 50, 55, 60 °C). b) Impedance of SEI on Cu foils. c) The activation energy for ion diffusion in Cu-SEI layer. d) Tafel plots and corresponding exchange current of Cu-SEI.

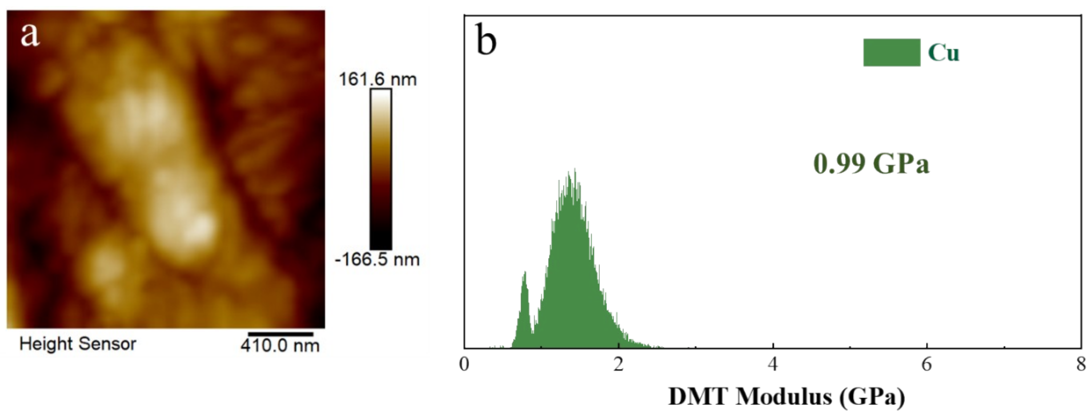

Figure S22. a) AFM images of the Cu current collector's surfaces. b) DMT modulus distribution of Cu-SEI.

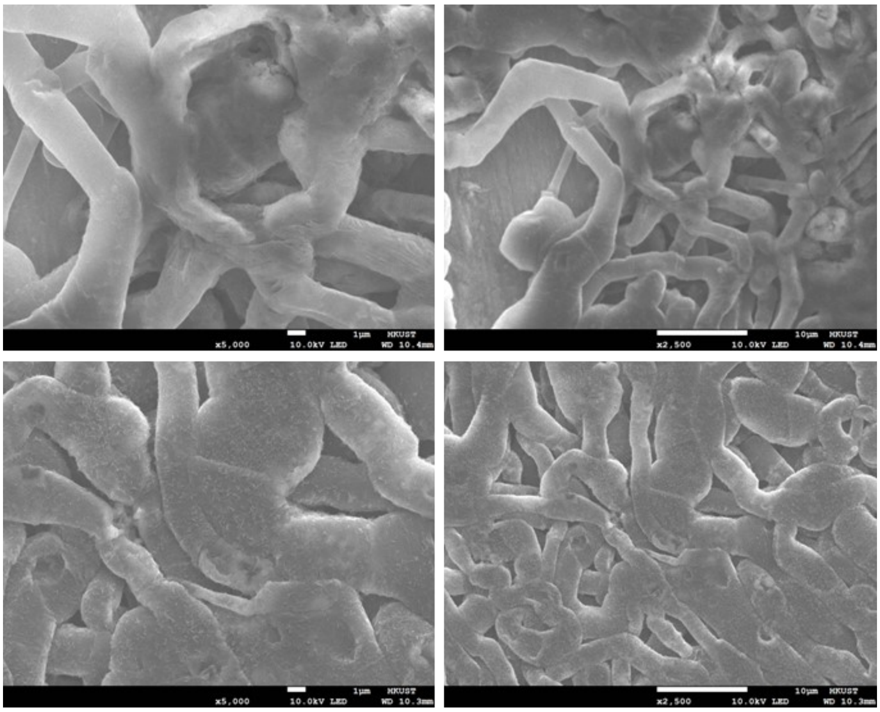

Figure S23. Lithium deposition morphologies on Cu current collector (with Cu-SEI).

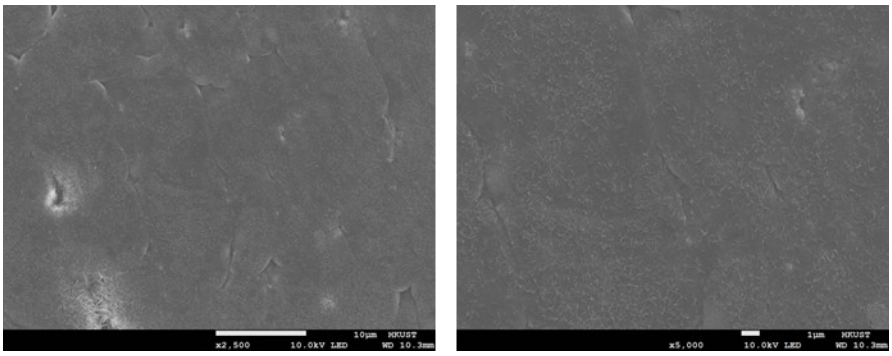

Figure S24. Lithium deposition morphologies on M-Ni after cycling tests (with MRIP-SEI).

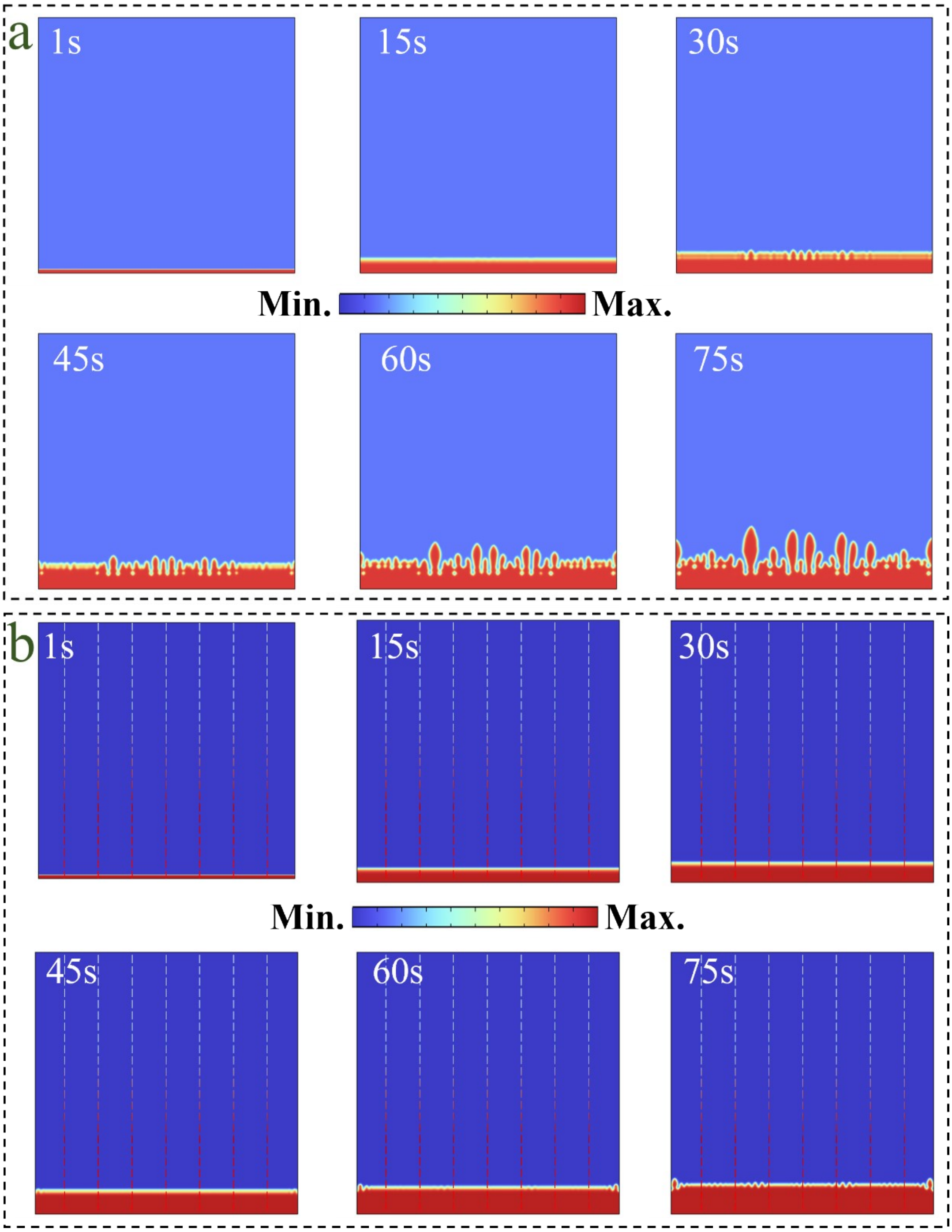

Figure S25. Phase field evolution of a) non-uniform nucleation and lithium deposition (Simulation of Ni-SEI), b) uniform nucleation and lithium deposition (Simulation of MRIP-SEI).

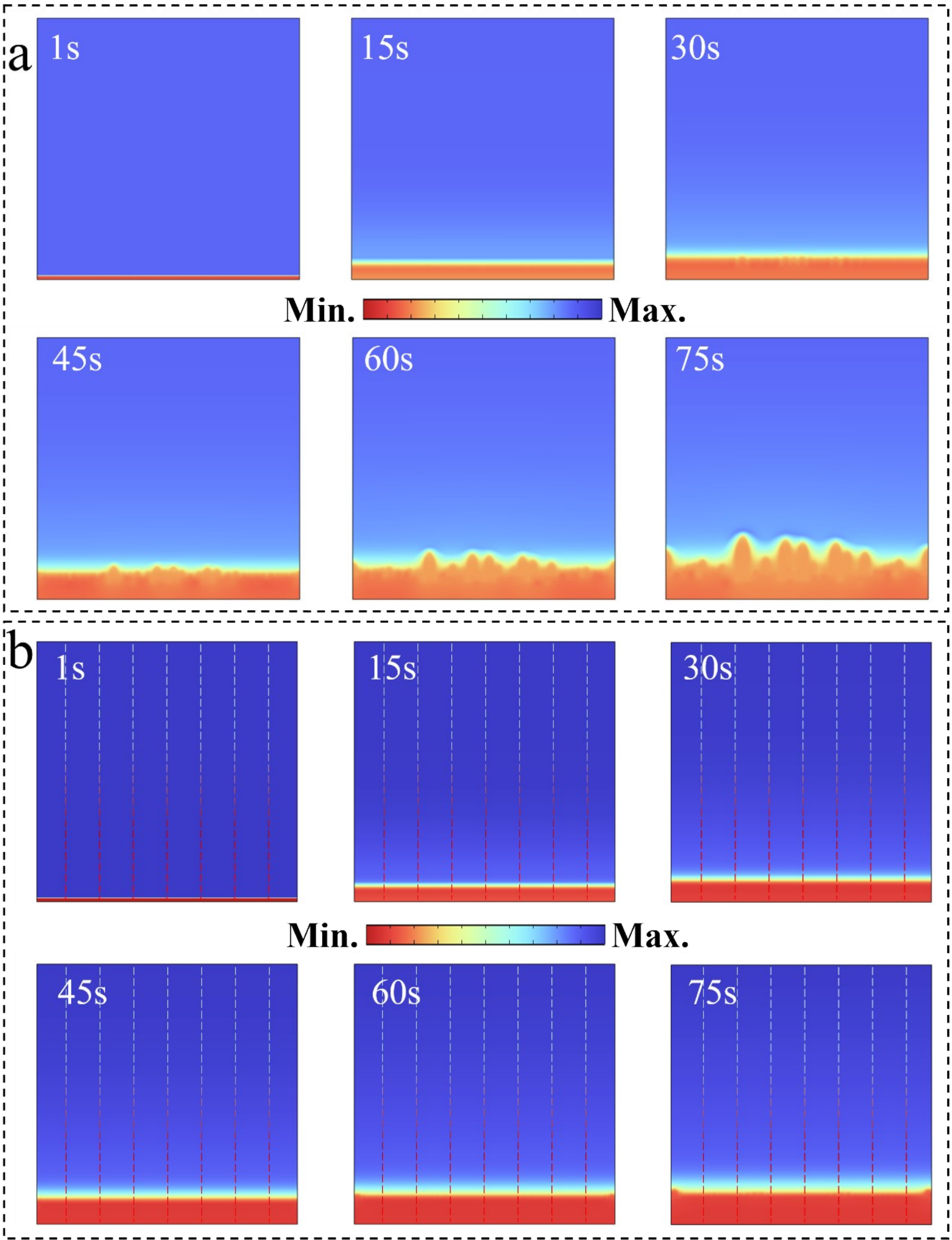

Figure S26. Concentration field evolution of a) non-uniform nucleation and lithium deposition (Simulation of Ni-SEI), b) uniform nucleation and lithium deposition (Simulation of MRIP-SEI).

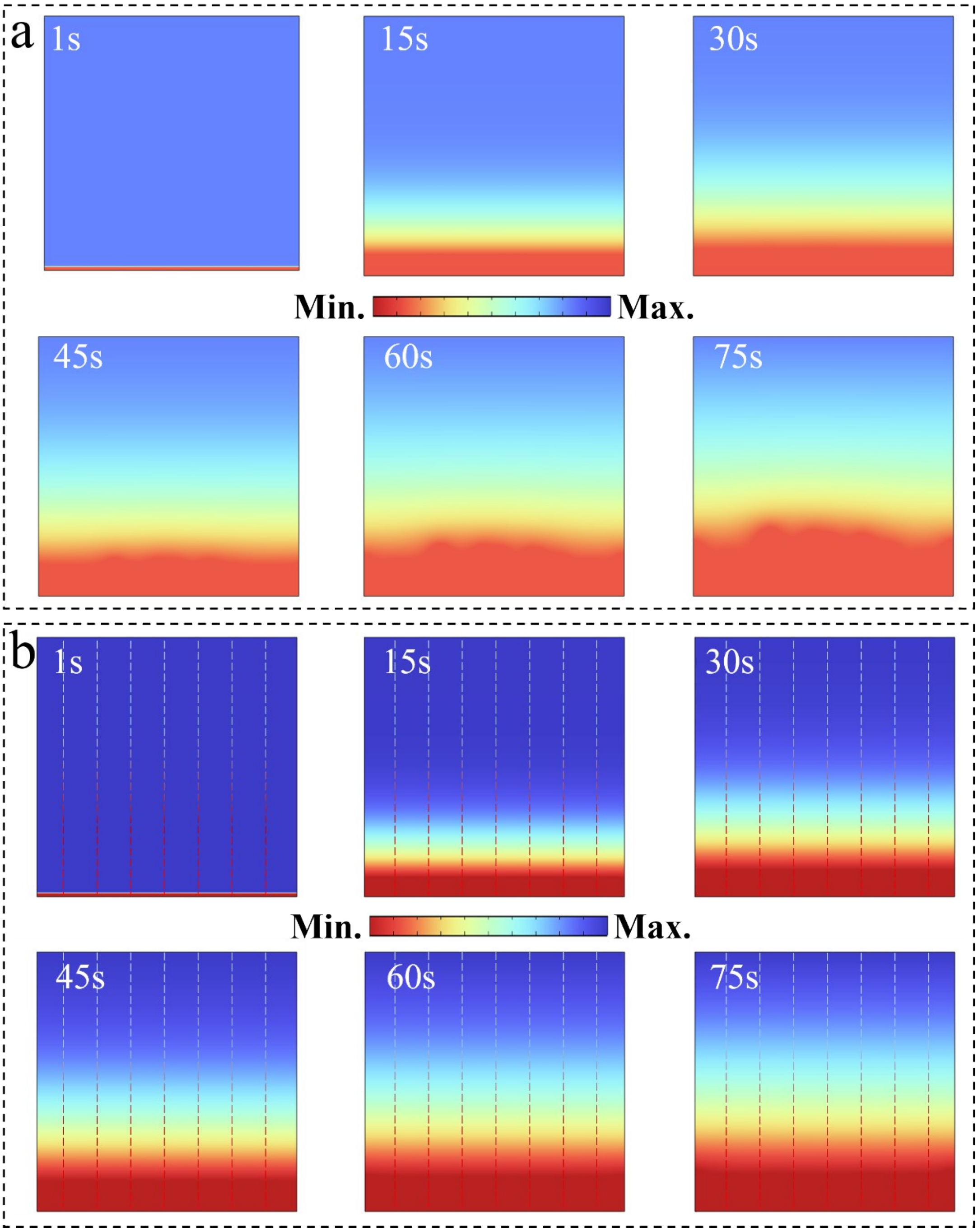

Figure S27. Potential field evolution of a) non-uniform nucleation and lithium deposition (Simulation of Ni-SEI), b) uniform nucleation and lithium deposition (Simulation of MRIP-SEI).

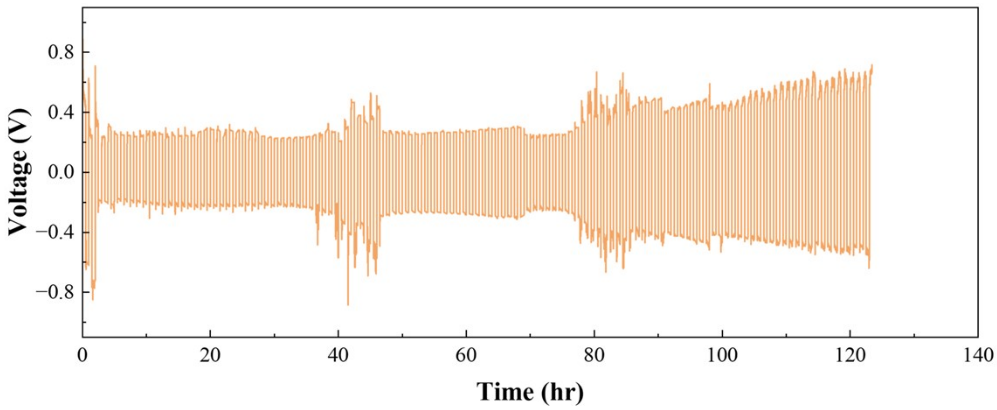

Figure S28. Cycling performance of Li|Li symmetrical cells at 2 mA cm^{-2} with Cu-SEI.

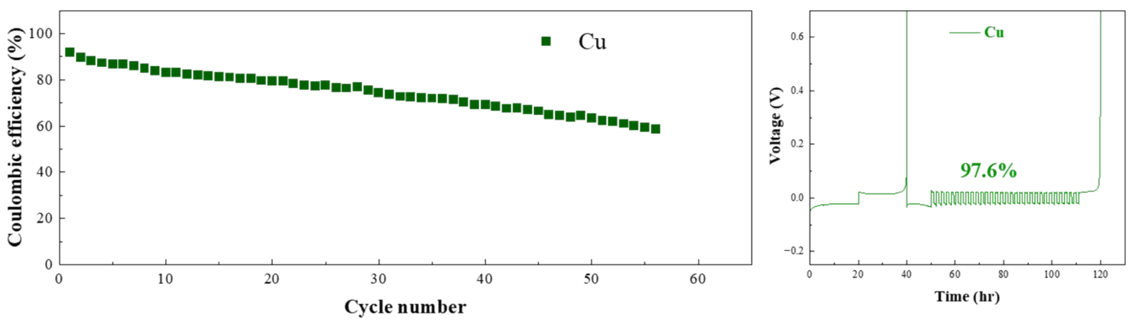

Figure S29. Cycle performance of Li|Cu cells at 0.5 mA cm^{-2} with Cu-SEI, and Aurbach average CE of Li|Cu cells at 2 mA cm^{-2} with Cu-SEI.

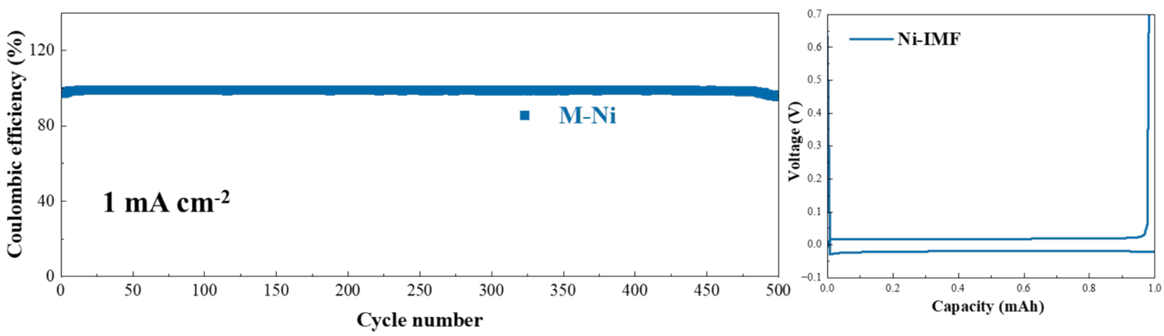

Figure S30. Cycle performance and charging/discharging curves of Li|Cu cell at 1 mA cm^{-2} with MRIP-SEI (M-Ni).

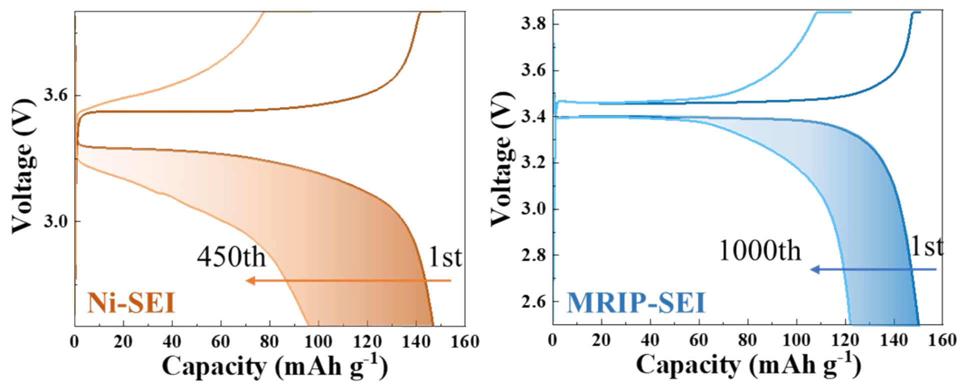

Figure S31. Charging/discharging curves of Cu@Li|LFP full cells at 0.5 C (N/P~0.8).

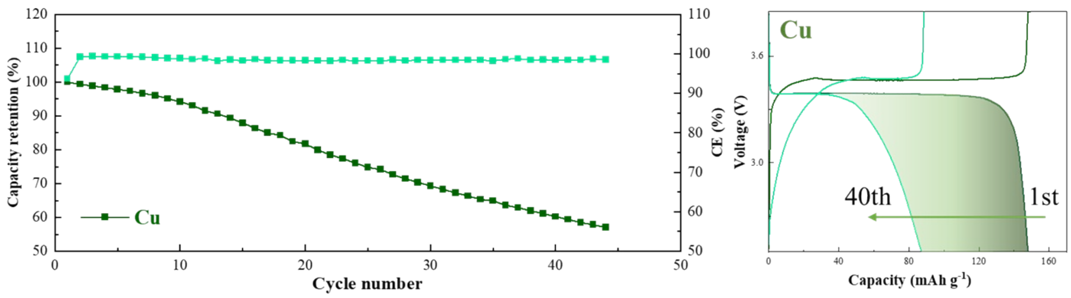

Figure S32. Cycling performance of Cu@Li|LFP full cells at 0.5 C (N/P~0.8) with Cu-SEI.

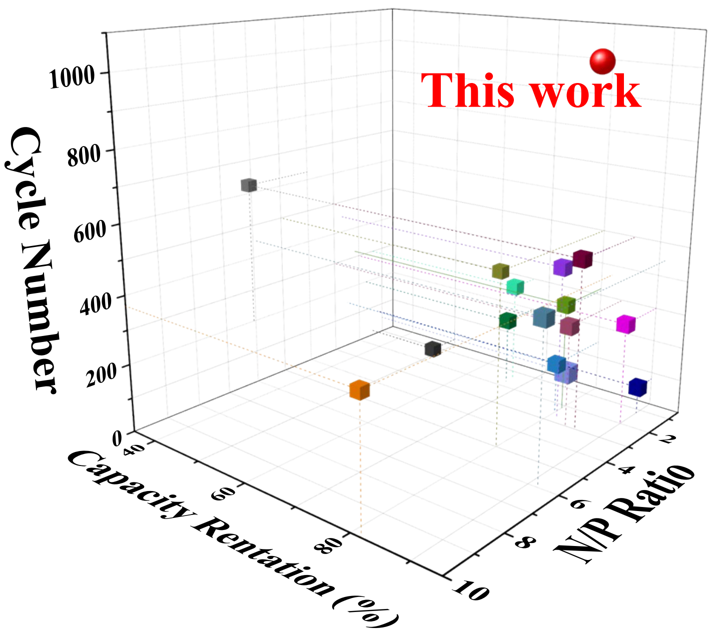

Figure S33. Performance comparison of LFP full cells with published literature.

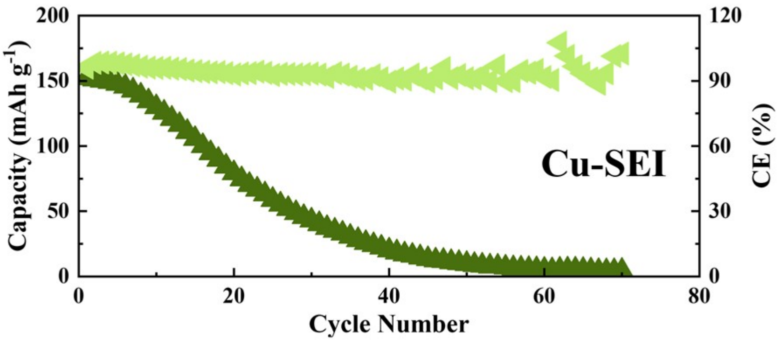

Figure S34. Cycling performance of anode-free Cu|LFP full cells at 0.3 C (N/P=0) with Cu-SEI.

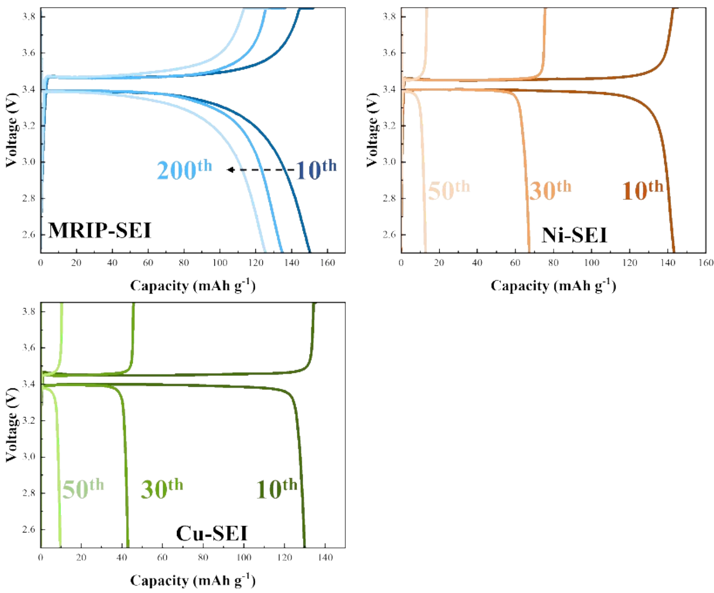

Figure S35. Charging/discharging curves of Cu|LFP full cells at 0.3 C (N/P=0).

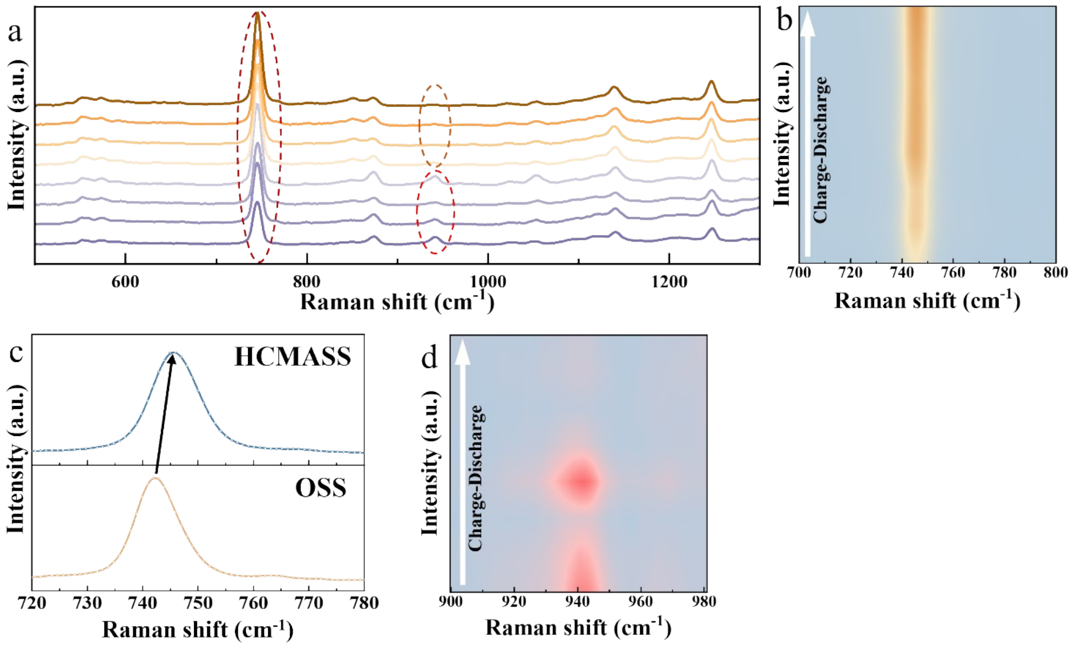

Figure S36. a) In-situ Raman curves on the cathode side during charging/discharging cycles with M-Ni. b) In-situ Raman spectra of Li^{+}-$TFSI^{-}$ during cycles with M-Ni. c) Raman spectra of $TFSI^{-}$ near cathode side with and without M-Ni. d) In-situ Raman spectra of DOL during cycles with M-Ni.

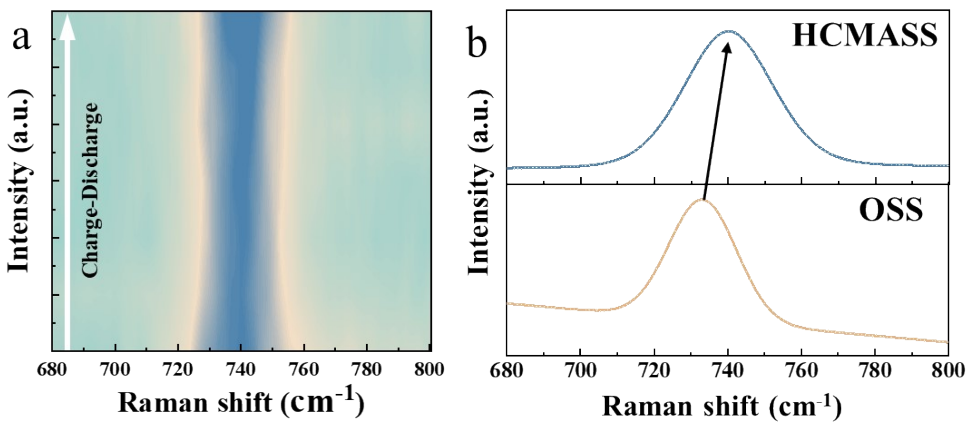

Figure S37. (a) In-situ Raman spectra of anions-cations in LHCEE during cycles with M-Ni. (b) Raman spectra of anions near cathode side in LHCEE with and without M-Ni.

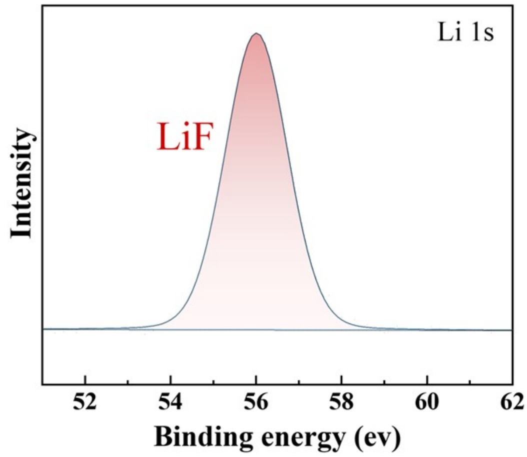

Figure S38. XPS spectra (Li 1s) of MRIP-CEI (M-Ni) after formation process.

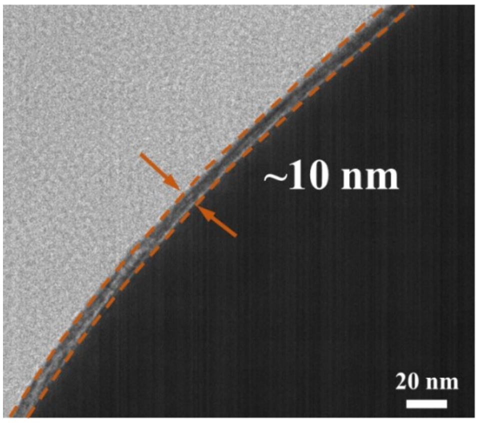

Figure S39. Cryo-TEM images of CEI morphology with M-Ni (MRIP-CEI) after the charge-discharge cycling test.

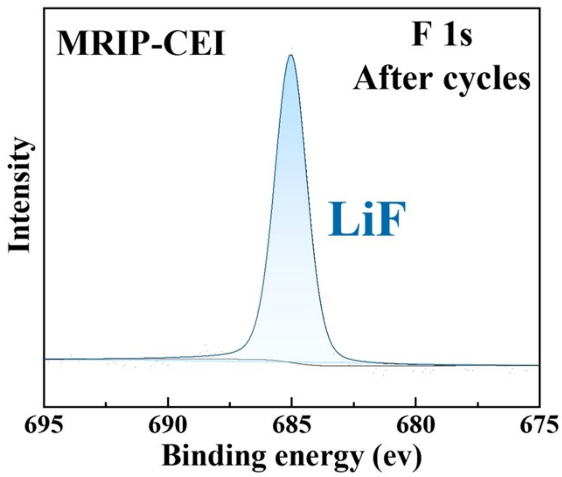

Figure S40. XPS spectra (F 1s) of MRIP-CEI (M-Ni) after the charge-discharge cycling test.

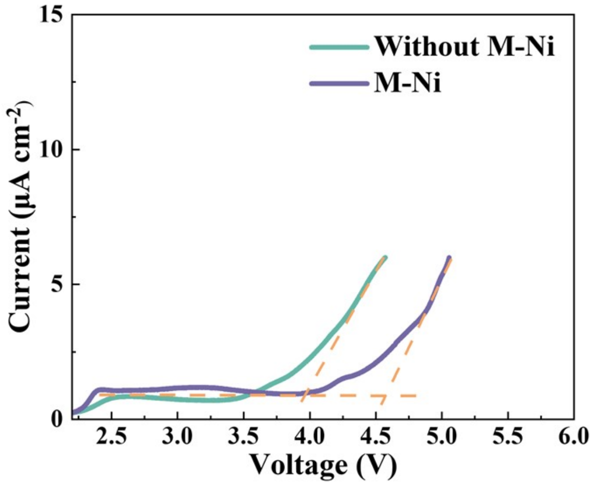

Figure S41. LSV curves with/without MRIP-CEI (M-Ni).

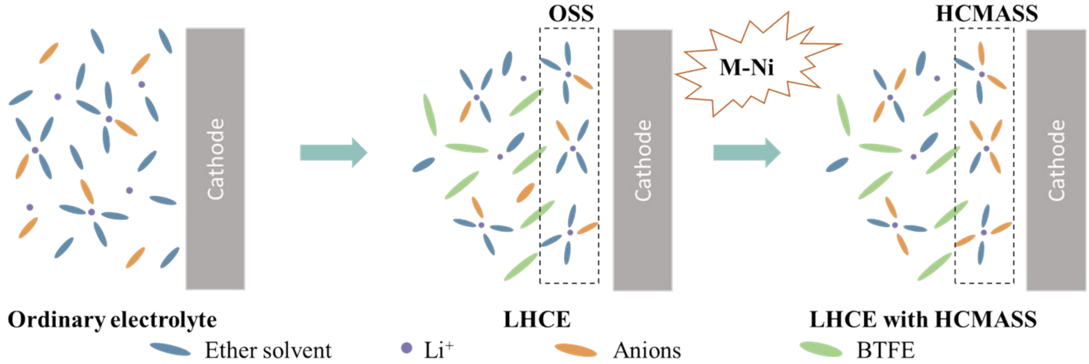

Figure S42. The schematic diagram illustrating the role of BTFE and its synergistic optimization of the cathode-electrolyte interface environment with M-Ni. (BTFE can be used as a diluent or inert solvent to increase the aggregation of solvated structures on the electrode surface in both the experimental and control cases. On this basis, the proposed helical migration strategy is employed to transform the ordinary solvation structures into HCMASS under the influence of M-Ni, thereby forming MRIP-CEI to improve high-voltage performance.)

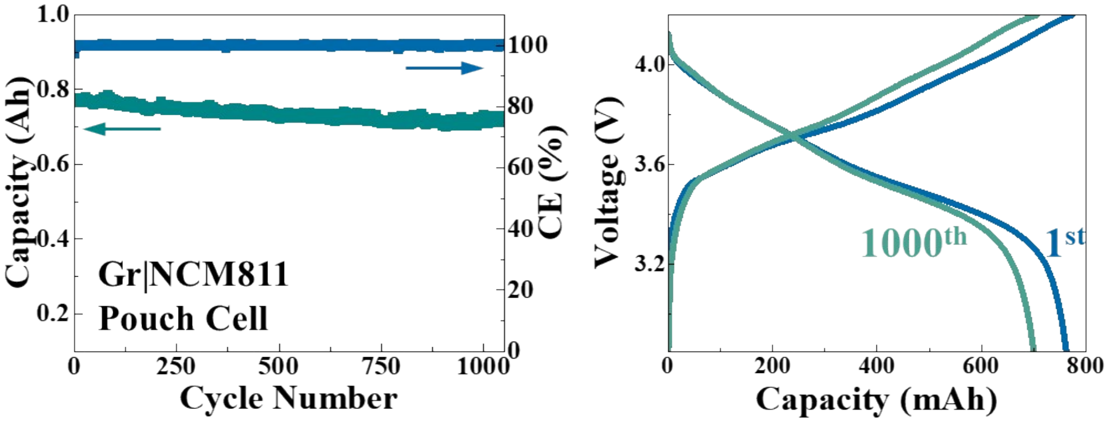

Figure S43. Cycling performance of Gr|NCM811 pouch cell with MRIP-CEI at 0.5 C.

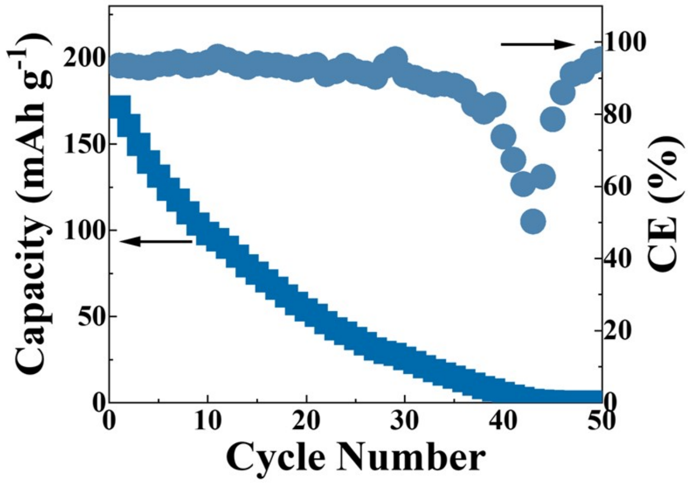

Figure S44. Cycling performance of Cu|NCM811 full cells at 0.5 C with Cu-SEI (2.8-4.3 V).

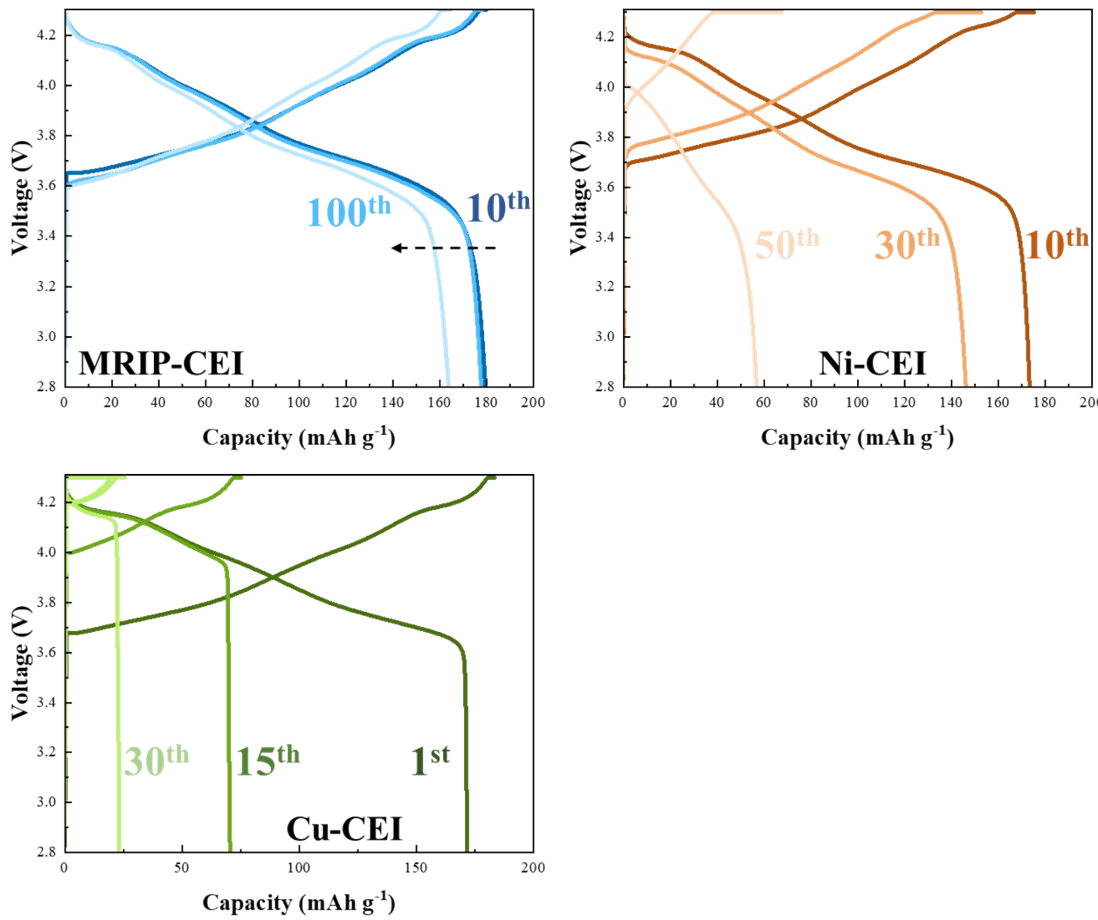

Figure S45. Charging/discharging curves of Cu|NCM811 full cells at 0.5 C (2.8-4.3 V).

Table S1 | Lattice information of different SEI inorganic species.

Species	**2-Theta**	**d (Å)**	**I (f)**	**(h k l)**	**Theta**	**1/(2d)**	**2pi/d**
LiF	38.713	2.324	90	(1 1 1)	19.357	0.2151	2.7036
LiF	44.996	2.013	100	(2 0 0)	22.498	0.2484	3.1213
Li_2O	33.613	2.664	100	(1 1 1)	16.807	0.1877	2.3586
Li_2S	31.24	2.8608	20	(2 0 0)	15.62	0.1748	2.1963
Li_3N	51.191	1.783	90	(1 1 0)	25.595	0.2804	3.5239

Table S2 | Performances of Li | Cu half cells.

Ref	Electrolyte	System	*I* (mA cm^{-2})	Cycle time	CE (%)
Nat. Energy[1]	1M LiTFSI-DEE:SFE	NGPE	0.5	200	99.4
Nat. Mater.[2]	1M $LiPF_6$-EC/DEC	$Sn(Oct)_2$	0.5	200	96
Nat. Commun.[3]	1M LiTFSI-DME/DOL (1:1)-2% $LiNO_3$	DF-PEG-DF	1	180	98.5
Nat. Commun.[4]	1.2M LPF-DFEA	DFEA	0.5	300	98.0
Nat. Commun.[5]	1.2m BMC+	BMC	0.5	125	99.3
Nat. Commun.[6]	1M LiPF6-EC/DMC/EMC	MADE-3	0.5	250	99.3
Sci. Adv.[7]	1M LiTFSI-DME/DOL (1:1)-5% $LiNO_3$	ED-Li	0.5	110	96
Nat. Commun.[8]	LiDFOB (0.6 M) and $LiBF_4$ (0.6 M) in FEC and DEC	YF_3	1	250	99.19
Nat. Commun.[9]	1M LiTFSI-DME/DOL (1:1)-1% $LiNO_3$	3D PI-clad	0.5	150	99
Sci. Adv.[10]	1M $LiPF_6$-EC/DMC/DEC-FEC	Ag/Li	0.1	100	94.6
Sci. Adv.[11]	1M LiTFSI-DME/DOL (1:1)-1% $LiNO_3$	Ag@CMF	1	120	98
Sci. Adv.[12]	1M LiTFSI-DME/DOL (1:1)-1% $LiNO_3$	NMMF-Cu	1	200	98.5
Adv. Energy Mater.[13]	1M LiTFSI-DME/DOL	b-Cu	0.5	100	89.66
Energy Storage Mater.[14]	1M $LiPF_6$-EC/DEC	$Cu(NO_3)_2$	0.5	50	90
Nano Energy[15]	1M $LiPF_6$-FEC/DMC	DEP	1	150	99.3
Angew. Chem.[16]	1M LiTFSI-DME/DOL (8:2)-3% $LiNO_3$	TEG-Cu	1	250	99.3
This work	1M LiTFSI-DOL/DME (1:1)-1%$LiNO_3$	HCMASS	1/0.5	1400/500	~98.6/98.9/99.9

Table S3 | Performances of LFP full cells.

Ref	Electrolyte	System	N/P ratio	Cycle time	Capacity retention (%)
Nat. Energy[17]	1 M LiFSI DEE and DOL/DME	SPAN	1	50	76
Adv. Mater.[18]	1 M LiFSI DOL/DME (1:1)	CMP-Li	2.5	150	80
Adv. Funct. Mater.[19]	1M LiTFSI-DOL/DME (1:1)-2%LiNO3	Li/SF-CuNW|LFP	1.4	300	67
Adv. Mater.[20]	1M LiTFSI-DME/DOL (1:1)-2% $LiNO_3$	Cu(220)	2.67	450	81.1
Sci. Adv.[21]	1M LiTFSI-DME/DOL (1:1)-1% $LiNO_3$	Li-Ag	5	500	80
Energy Storage Mater.[22]	1M LiTFSI-DME/DOL (1:1)-2% $LiNO_3$	LiF/Li_xMg_y layer	5.9	450	91.2
Adv. Funct. Mater.[23]	LiTFSI-MPEGMA-PFEMA-PUMA	FELMA	2.17	320	80
Angew. Chem.[24]	1M LiTFSI-DME/DOL (1:1)-1% $LiNO_3$	TPMS	3	500	13
Small[25]	1M LiTFSI-DME/DOL (1:1)-2% $LiNO_3$	PPY	1.5	20	50
Energy Storage Mater.[26]	1M LiTFSI-DME/DOL (1:1)-1% $LiNO_3$	FGLi	1.7	200	67
Adv. Funct. Mater.[27]	1M LiTFSI-DME/DOL (1:1)-1% $LiNO_3$	Ag@CNF	2	300	90
Adv. Energy Mater.	1M LiTFSI-DME/DOL (1:1)-2% $LiNO_3$	LZ-rGO	1.2	80	>90
Nat. Commun[28]	1M LiTFSI-DME/DOL (1:1)-2% $LiNO_3$	ZDDP	14.1	370	81.9
Nat. Commun[29]	Ether-based electrolyte	DDE-PN	3	300	84
This work	1M LiTFSI-DOL/DME (1:1)-1%$LiNO_3$	HCMASS	0.8	1000	>80%

1. Y. Meng, D. Zhou, R. Liu, Y. Tian, Y. Gao, Y. Wang, B. Sun, F. Kang, M. Armand, B. Li, G. Wang and D. Aurbach, *Nature Energy*, 2023, **8**, 1023-1033.
2. J. Shi, T. Koketsu, Z. Zhu, M. Yang, L. Sui, J. Liu, M. Tang, Z. Deng, M. Liao, J. Xiang, Y. Shen, L. Qie, Y. Huang, P. Strasser and J. Ma, *Nature Materials*, 2024, DOI: 10.1038/s41563-024-01997-8.
3. Q.-K. Zhang, X.-Q. Zhang, J. Wan, N. Yao, T.-L. Song, J. Xie, L.-P. Hou, M.-Y. Zhou, X. Chen, B.-

Q. Li, R. Wen, H.-J. Peng, Q. Zhang and J.-Q. Huang, *Nat. Energy*, 2023, **8**, 725-735.
4. Y. Wang, S. Dong, Y. Gao, P.-K. Lee, Y. Tian, Y. Meng, X. Hu, X. Zhao, B. Li, D. Zhou and F. Kang, *Nat. Commun.*, 2024, **15**, 5408.
5. J. Chen, D. Zhang, L. Zhu, M. Liu, T. Zheng, J. Xu, J. Li, F. Wang, Y. Wang, X. Dong and Y. Xia, *Nature Communications*, 2024, **15**, 3217.
6. Z. Cui, Z. Jia, D. Ruan, Q. Nian, J. Fan, S. Chen, Z. He, D. Wang, J. Jiang, J. Ma, X. Ou, S. Jiao, Q. Wang and X. Ren, *Nature Communications*, 2024, **15**, 2033.
7. S. Zhang, Y. Li, L. J. Bannenberg, M. Liu, S. Ganapathy and M. Wagemaker, *Science Advances*, 2024, **10**, eadj8889.
8. Y. Zhang, R. Qiao, Q. Nie, P. Zhao, Y. Li, Y. Hong, S. Chen, C. Li, B. Sun, H. Fan, J. Deng, J. Xie, F. Liu and J. Song, *Nat. Commun.*, 2024, **15**, 4454.
9. P. Zou, Y. Wang, S.-W. Chiang, X. Wang, F. Kang and C. Yang, *Nature Communications*, 2018, **9**, 464.
10. C.-H. Zhang, Y.-J. Guo, S.-J. Tan, Y.-H. Wang, J.-C. Guo, Y.-F. Tian, X.-S. Zhang, B.-Z. Liu, S. Xin, J. Zhang, L.-J. Wan and Y.-G. Guo, *Sci. Adv.*, 2024, **10**, eadl4842.
11. Y. Fang, S. L. Zhang, Z.-P. Wu, D. Luan and X. W. Lou, *Sci. Adv.*, 2021, **7**, eabg3626.
12. H. Yuan, J. Nai, H. Tian, Z. Ju, W. Zhang, Y. Liu, X. Tao and X. W. Lou, *Science Advances*, 2020, **6**, eaaz3112.
13. S. Pyo, S. Ryu, Y. J. Gong, J. Cho, H. Yun, H. Kim, J. Lee, B. Min, Y. Choi, J. Yoo and Y. S. Kim, *Advanced Energy Materials*, 2023, **13**, 2203573.
14. R. Zhao, X. Li, Y. Si, S. Tang, W. Guo and Y. Fu, *Energy Storage Materials*, 2021, **37**, 1-7.
15. H. Su, P. Liu, Y. Liu, S. Liu, Y. Zhong, X. Xia, X. Wang and J. Tu, *Nano Energy*, 2023, **115**, 108722.
16. Y. Wang, Z. Qu, S. Geng, M. Liao, L. Ye, Z. Shadike, X. Zhao, S. Wang, Q. Xu and B. Yuan, *Angewandte Chemie*, 2023, **135**, e202304978.
17. J. Holoubek, H. Liu, Z. Wu, Y. Yin, X. Xing, G. Cai, S. Yu, H. Zhou, T. A. Pascal, Z. Chen and P. Liu, *Nat. Energy*, 2021, **6**, 303-313.
18. K. Zhang, W. Liu, Y. Gao, X. Wang, Z. Chen, R. Ning, W. Yu, R. Li, L. Li, X. Li, K. Yuan, L. Ma, N. Li, C. Shen, W. Huang, K. Xie and K. P. Loh, *Adv. Mater.*, 2021, **33**, 2006323.
19. A. Fu, C. Wang, J. Peng, M. Su, F. Pei, J. Cui, X. Fang, J.-F. Li and N. Zheng, *Adv. Funct. Mater.*, 2021, **31**, 2009805.
20. J. Zhan, L. Deng, Y. Liu, M. Hao, Z. Wang, L.-T. Dong, Y. Yang, K. Song, D. Qi, J. Wang, S. Wang, H. Liu, W. Zhou and H. Chen, *Adv. Mater.*, 2025, **37**, 2413420.
21. Z. Wang, J. Xia, X. Ji, Y. Liu, J. Zhang, X. He, W. Zhang, H. Wan and C. Wang, *Nat. Energy*, 2024, **9**, 251-262.
22. J. Jiang, X. Hu, S. Lu, C. Shen, S. Huang, X. Liu, Y. Jiang, J. Zhang and B. Zhao, *Energy Storage Mater.*, 2023, **54**, 885-894.
23. A. Wang, Y. Nie, Y. Zhao, D. Xu, L. Zhang, Z. Zhao, L. Ren, S. Zhou, X. Liu and J. Luo, *Adv. Funct. Mater.*, 2024, **34**, 2401462.
24. C. Ma, S. Zou, Y. Wu, K. Yue, X. Cai, Y. Wang, J. Nai, T. Guo, X. Tao and Y. Liu, *Angew. Chem.*, 2024, **136**, e202402910.
25. C. Xie, C. Zhao, H. Jeong, Q. Liu, T. Li, W. Xu, L. Cheng, G.-L. Xu, K. Amine and G. Chen, *Small*, 2024, **20**, 2306868.
26. P. Xu, X. Hu, X. Liu, X. Lin, X. Fan, X. Cui, C. Sun, Q. Wu, X. Lian, R. Yuan, M. Zheng and Q.

Dong, *Energy Storage Mater.*, 2021, **38**, 190-199.
27. A. Huang, H. Huang, S. Li, X. Pan, S. Sun, X. Su, H. Geng, L. Li, M. Maximov, J. Ren and S. Peng, *Adv. Funct. Mater.*, 2025, **n/a**, 2506258.
28. S. Huang, Z. Wu, B. Johannessen, K. Long, P. Qing, P. He, X. Ji, W. Wei, Y. Chen and L. Chen, *Nat. Commun.*, 2023, **14**, 5678.
29. W. Zhang, Y. Lu, Q. Feng, H. Wang, G. Cheng, H. Liu, Q. Cao, Z. luo, P. Zhou, Y. Xia, W. Hou, K. Zhao, C. Du and K. Liu, *Nat. Commun.*, 2025, **16**, 3344.